Journal of
Applied Crystallography
ISSN 0021-8898
Editor: **Anke R. Kaysser-Pyzalla**

A model for calculating diffraction elastic constants

Thomas Gnäupel-Herold, Adam A. Creuziger and Mark Iadicola

J. Appl. Cryst. (2012). **45**, 197–206

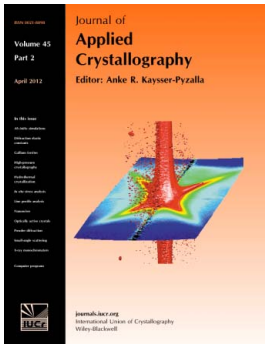

Journal of
Applied Crystallography
ISSN 0021-8898

Received 25 August 2011
Accepted 18 January 2012

A model for calculating diffraction elastic constants

Thomas Gnäupel-Herold,[a,b]* Adam A. Creuziger[c] and Mark Iadicola[c]

[a]Materials Science and Engineering, University of Maryland, Building 090, Room 2135, College Park, MD 20742, USA, [b]Center for Neutron Research, NIST, 100 Bureau Drive, Stop 6102, Gaithersburg, MD 20899-6102, USA, and [c]Metallurgy Division, NIST, 100 Bureau Drive, Stop 8553, Gaithersburg, MD 20899-8553, USA. Correspondence e-mail: tg-h@nist.gov

A model, dubbed the inverse Kröner model, is proposed to calculate the diffraction elastic constants from the elastic constants of a single crystal. It is related to the classic Kröner model, and both are identified as bounds on the diffraction elastic constants. Through the grain shape as controlling parameter, the classic Kröner model is bound by the *hkl*-independent mechanical limit given by the bulk elastic constants of the matrix, while the inverse Kröner model approaches the Reuss limit.

1. Introduction

Diffraction elastic constants (DECs) provide a relationship between elastic lattice strains and macroscopic stress. As such, they form the basis of diffractive stress determination. The models used for the calculation of DECs have undergone a very long development from the Reuss model (Möller & Martin, 1939), the Reuss–Voigt average, as suggested by Hill (Hill, 1952), the Kröner model (Bollenrath *et al.*, 1967; Behnken & Hauk, 1986), and, more recently, the use of perturbation theory by de Wit (1997). First and foremost, DECs depend on the Miller indices (*hkl*) of the reflection used for measuring the lattice spacings. Secondly, from Eshelby's theory (Eshelby, 1961) it is known that the strain/stress response of a single grain depends on the elastic properties of its surroundings as well as its shape. Prominent examples where these interactions come into play are composites of hard particles that reinforce an elastically soft matrix. DECs are orientation-selective averages over a subset of all grains, and therefore these dependencies remain valid to a degree. Thirdly, it is known from various experimental results (Barral *et al.*, 1987; Brakman & Penning, 1988; Dölle *et al.*, 1977, 1978; Baczmanski *et al.*, 1993; Dölle, 1979; Hauk, 1997) that preferred orientation of grains can have a profound effect on the magnitude and orientation dependence of DECs. Consequently, one should expect that DECs themselves depend on these factors. The Kröner theory is the only model that can account for all of these effects, yet the literature shows that, because of the relative simplicity of the calculations and despite their shortcomings, the Reuss model and the Reuss–Voigt average are used predominantly. For isotropic aggregates and multiphase polycrystals in which the elastic properties of the constituents are not too dissimilar, the Reuss–Voigt average and the Kröner model yield results in acceptable to good agreement with measured DECs. Other models such as the modified Voigt model (Murray & Noyan, 1999), de Wit's model and the geometric average (Baczmanski *et al.*, 1993; Moraviec, 1989; Matthies & Humbert, 1993) have not yet been compared with experimental results on a wider scale. There are relatively few comparative data for materials with preferred orientation, partly because the techniques used to compare experimental results vary widely. For example, recalculated stresses are sometimes compared with a known applied stress, thus reducing the quality measure of the DEC model used to a single number comparison. A comparison of angular distributions of measured and recalculated lattice strains has considerably more detail to offer but it also has to reproduce the magnitude of the applied stress. A more appropriate comparison can be gleaned from measured DECs themselves. However, measuring DECs requires a large number of measurements because lattice strains have to be measured for different tilt angles ψ and azimuth angles φ, as well as for several applied stresses. This type of relationship is conveniently expressed as stress factors F_{ij}. An alternative expression for F_{ij} is developed in the following.

2. Theoretical considerations

The stress factors (Dölle *et al.*, 1977, 1978; Dölle, 1979; Barral *et al.*, 1987; Hauk, 1997; Koch *et al.*, 2004; Ortner, 2006) are defined as

$$\varepsilon(\varphi, \psi, hkl) = \frac{d(\varphi, \psi, hkl) - d_0(\varphi, \psi, hkl)}{d_0(\varphi, \psi, hkl)} = \frac{\partial \varepsilon(\varphi, \psi, hkl)}{\partial \overline{\sigma}_{ij}} \overline{\sigma}_{ij} = F_{ij}(\varphi, \psi, hkl)\overline{\sigma}_{ij}, \quad (1)$$

where $\varepsilon(\varphi, \psi, hkl)$ is the average lattice strain of all grains oriented such that their lattice planes (*hkl*) contribute to the diffracted intensity in the direction given by the azimuth φ and tilt angle ψ. Note that the reference d spacing $d_0(\varphi, \psi, hkl)$ may depend on the orientation as well, as is the case for samples with residual stresses from plastic deformation. The $\overline{\sigma}_{ij}$ parameters are the stresses that pertain to the macroscopic aggregate. For isotropic materials without preferred orientation, F_{ij} is related to the traditionally used DECs s_1 and $\frac{1}{2}s_2$ through (Hauk, 1997)

$$F_{ij} = \begin{pmatrix} s_1 + \frac{1}{2}s_2\cos^2\varphi\sin^2\psi & \frac{1}{2}\frac{1}{2}s_2\sin 2\varphi\sin^2\psi & \frac{1}{2}\frac{1}{2}s_2\cos\varphi\sin 2\psi \\ \frac{1}{2}\frac{1}{2}s_2\sin 2\varphi\sin^2\psi & s_1 + \frac{1}{2}s_2\sin^2\varphi\sin^2\psi & \frac{1}{2}\frac{1}{2}s_2\sin\varphi\sin 2\psi \\ \frac{1}{2}\frac{1}{2}s_2\cos\varphi\sin 2\psi & \frac{1}{2}\frac{1}{2}s_2\sin\varphi\sin 2\psi & s_1 + \frac{1}{2}s_2\cos^2\psi \end{pmatrix}. \quad (2)$$

The coordinate system used in the following is shown in Fig. 1.

In the following, Kröner's notation is adopted, in which fourth-rank tensors are denoted by upper case letters if they refer to properties of the overall composite (matrix), and lower case letters are used for the orientation-dependent properties of the grains. Also, this discussion extends to composites of noncrystalline and diffracting crystalline materials (grains) with known elastic properties. The grains in the composite are described by an ellipsoidal shape with an orientation ω of the ellipsoid axes. Furthermore, they are characterized by their stiffness $c_{ijkl}(g)$ and compliance $s_{ijkl}(g)$, which depend on the orientation g of the crystal lattice with respect to the specimen frame. A fourth-rank tensor dependent on the orientation g is expressed as

$$a_{ijkl}(g) = g^{-1}_{im}g^{-1}_{jn}g^{-1}_{ko}g^{-1}_{lp}a_{mnop}, \quad (3)$$

in which a_{mnop} is the property tensor in the crystal reference frame, $a_{ijkl}(g)$ is the tensor in the specimen system and g_{ij} is the transformation matrix [using Bunge angles $(\varphi_1, \phi, \varphi_2)$] for the transformation from the specimen reference frame to the crystal reference frame (Bunge, 1982).

$$g\{\varphi_1\phi\varphi_2\} = \begin{pmatrix} \cos\varphi_1\cos\varphi_2 - \sin\varphi_1\sin\varphi_2\cos\phi & \sin\varphi_1\cos\varphi_2 + \cos\varphi_1\sin\varphi_2\cos\phi & \sin\varphi_2\sin\phi \\ -\cos\varphi_1\sin\varphi_2 - \sin\varphi_1\cos\varphi_2\cos\phi & -\sin\varphi_1\sin\varphi_2 + \cos\varphi_1\cos\varphi_2\cos\phi & \cos\varphi_2\sin\phi \\ \sin\varphi_1\sin\phi & -\cos\varphi_1\sin\phi & \cos\phi \end{pmatrix}. \quad (4)$$

Note that equation (3) uses the inverse of g because the transformation is from the crystal frame to the specimen frame. The overall elastic constants of the composite, C_{ijkl} and S_{ijkl}, are considered as known. The strain and stress in a single crystallite depend on the orientation and shape of the crystallite. The relationship between the strain $\varepsilon_{ij}(g)$ and stress $\sigma_{ij}(g)$ of a single grain and the macroscopic stress $\overline{\sigma}_{ij}$ and strain $\overline{\varepsilon}_{ij}$ according to Kröner (1958) and Kneer (1965) is expressed through the transfer tensors p and q:

$$\sigma_{ij}(g) = p_{ijkl}(g, \omega)\,\overline{\varepsilon}_{kl}, \quad (5)$$

$$\varepsilon_{ij}(g) = q_{ijkl}(g, \omega)\,\overline{\sigma}_{kl}. \quad (6)$$

Appropriate averaging of equation (6) yields the Kröner model. Because of the difficulties associated with the determination of the distribution of the grain ellipsoid-axis orientations ω (not to be confused with the crystallite orientation distribution), it is assumed in the following that the ellipsoid axes (a_1, a_2, a_3) align with (RD, TD, ND) (defined in Fig. 1), and average values for the ellipsoid axis aspect ratios will be used, where appropriate. Through Hooke's law one has the relationship

$$p_{ijkl}(g) = c_{ijmn}(g)\,q_{mnop}(g)\,C_{opkl}. \quad (7)$$

However, it will be shown in the following that it is advantageous to consider the inverse tensor $p^{-1}_{ijkl}(g)$ instead, where the superscript indicates the inverse fourth-rank tensor. It is obvious that, in general, $p^{-1}_{ijkl}(g) \neq q_{ijkl}(g)$ which, when averaged over all orientations, was shown by Kröner (1958) to represent bounds on the overall elastic constants of the polycrystal in the form

$$\overline{q}_{ijkl} < S_{ijkl} < \overline{p}^{-1}_{ijkl} \quad \text{or} \quad \overline{q}_{ijkl} > S_{ijkl} > \overline{p}^{-1}_{ijkl}, \quad (8)$$

where the inequalities indicate that $\overline{q}_{ijkl}$ and $\overline{p}^{-1}_{ijkl}$ can be either an upper or a lower bound, depending on the single-crystal constants, grain shape and orientation distribution. Furthermore, it was shown by Kröner (1958) and Kneer (1965) that spherical grains or ellipsoids with randomly oriented axes averaged over all crystal orientations yield $\overline{q}_{ijkl} = \overline{p}^{-1}_{ijkl}$. It must be pointed out that, because the orientation average for DECs is not complete and involves only a small subset of grain orientations, the DECs are generally subject to a relationship of the type given by equation (8). The often-used Kröner model is therefore only one of two possible formulae, and one can express a relationship between lattice strain and macroscopic stress entirely equivalent to equation (6) as

$$\varepsilon(g) = \overline{p}^{-1}_{ijkl}(g)\overline{\sigma}_{kl}, \quad (9)$$

which in the following is referred to as the inverse Kröner model because the inverse of tensor $p(g)$ is used. Kröner (1958) derived expressions that define $p_{ijkl}(g)$ and $q_{ijkl}(g)$:

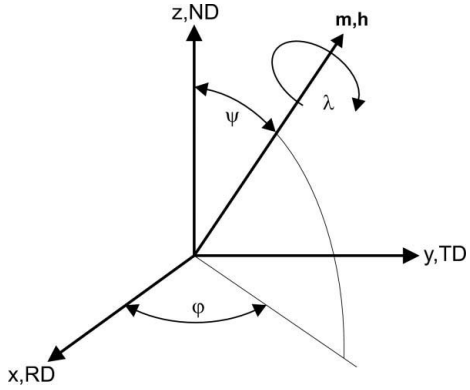

Figure 1
Specimen reference frame with measurement direction **m**||**h**, where **h** is the direction normal to the lattice planes (*hkl*) that contribute to a reflection in the measurement direction **m** given by the spherical polar angles φ and ψ. The direction **h** is defined in the Cartesian crystal reference frame (not shown) by spherical polar angles Φ_B and β_B. RD is the rolling direction, TD is the transverse direction and ND is the direction normal to the sheet plane. The base vectors of the Cartesian system must be chosen in accordance with the system used in the measurement of the single-crystal elastic constants.

$$p_{ijkl}(g) = C_{ijkl} + r_{ijkl}(g), \quad q_{ij}(g) = S_{ijkl} + t_{ijkl}(g), \tag{10}$$

$$r_{ijkl}(g) = c_{ijkl}(g) - C_{ijkl} + c_{ijmn}(g)\, u_{mnkl}(g), \tag{11}$$

$$t_{ijkl}(g) = u_{ijmn}(g)\, S_{mnkl}, \tag{12}$$

$$u_{ijkl}(g) = v^{-1}_{ijmn}(g)\,[c_{mnkl}(g) - C_{mnkl}], \tag{13}$$

$$v_{ijkl}(g) = c_{ijkl}(g) - C_{ijkl} + C_{ijmn} w_{mnkl}, \tag{14}$$

where $c_{ijkl}(g)$ is the stiffness tensor of the crystallite, C_{ijkl} and S_{ijkl} are, respectively, the stiffness and compliance tensors of the overall composite, and w_{ijkl} is the inverse Eshelby tensor (Kinoshita & Mura, 1971; Mura, 1987; Gavazzi & Lagoudas, 1990). From equation (10), Kröner established the conditions for calculating the overall elastic constants

$$\overline{r(g)} = 0 \quad \text{and} \quad \overline{t(g)} = 0, \tag{15}$$

where the overbars indicate the average over all crystal orientations. Note that $r(g)$ and $t(g)$ represent different physical quantities, where $r(g)$ is determined in units of GPa and $t(g)$ in units of GPa^{-1}. Equations (15) yield two solutions, $C^{(r)}$ and $C^{(t)}$, that are not necessarily equal. As indicated before, both yield the same solution only if the grains are all spherical or ellipsoids with randomly oriented axes. Similar to the Reuss and Voigt bounds but not as straightforward, the existence of two solutions, $C^{(r)}$ and $C^{(t)}$, is to be interpreted as bounds on the overall elastic moduli. The existence of bounds is rooted in the condition of continuity of displacement (fulfilled for Voigt) and equilibrium of traction (fulfilled for Reuss) at the grain–matrix interface for all grains. If the polycrystal under consideration were to consist of needle-shaped grains aligned in the same direction, then the elastic moduli may be closer to the Voigt bound in the direction of the longitudinal axis, while Reuss bounds may be closer for flat platelet grains with their short axis aligned in the same direction.

In the case of DECs, one must calculate partial orientation averages in the sense that only those orientations contribute to the average for which a given crystal direction **h** is parallel to a given sample direction **m**. In this case, one has both $\overline{r(g)}^{m\|h} \neq 0$ and $\overline{t(g)}^{m\|h} \neq 0$, with the consequence that

$$S + \overline{t(g)}^{m\|h} \neq \left[C + \overline{r(g)}^{m\|h}\right]^{-1}. \tag{16}$$

In fact, the whole basis of the Kröner model for DEC calculation is $\overline{t(g)}^{m\|h} \neq 0$. From equation (16), together with equations (11) and (12), it can be concluded that the only general exception to the inequality (16) is when both $c(g) = C$ for all orientations g. In other words, the grains have to be elastically isotropic (tungsten comes to mind). For all other cases, DECs calculated using the Kröner model or the inverse Kröner model [first and second parts of equation (10)] will be different from each other, except for singular combinations of grain shape and grain orientation (see discussion in §3.1 below).

Using a compact notation without indices, equation (9), which is also the right-hand side of equation (16), can now be written as

$$\begin{aligned}\varepsilon(g) &= p^{-1}(g)\overline{\sigma} \\ &= \left\{c(g) + c(g)[c(g) - C + Cw]^{-1}[c(g) - C]\right\}^{-1}\overline{\sigma}.\end{aligned} \tag{17}$$

As shown previously (Barral *et al.*, 1987; Brakman & Penning, 1988; Dölle *et al.*, 1977, 1978; Baczmanski *et al.*, 1993; Dölle, 1979; Hauk, 1997; Pina *et al.*, 1997; Van Houtte & De Buyser, 1993), the quantity that is measurable by diffraction is that which is in the direction of the z axis of an intermediate reference frame. The z axis of this intermediate coordinate system is parallel to both the direction given by the tilt and azimuth angles (ψ, φ) in the specimen coordinate system and the direction **h** [normal to the diffracting lattice planes (hkl)] in the fixed crystal coordinate system.

$$\varepsilon^{\mathrm{L}}_{33} = \varepsilon(\varphi, \phi, hkl) = \overline{p^{-1}_{33kl}(g^{\mathrm{L}}, \omega)}\,\overline{\sigma}_{kl}, \tag{18}$$

where the overbar signifies that the orientation average is taken over rotations about **h** for grains with the direction **h** parallel to (ψ, φ). The transformation matrix g^{L} is given by (Bunge, 1982)

$$g^{\mathrm{L}} = g_2\left\{\lambda, \Phi_{\mathrm{B}}, \frac{\pi}{2}, -\beta_{\mathrm{B}}\right\} g_1\left\{\varphi + \frac{\pi}{2}, \psi, 0\right\}, \tag{19}$$

as the product of the transformation g_1 from the specimen coordinate system to the intermediate system and g_2 as the transformation from the intermediate system to the fixed crystal coordinate system. The inverse of g^{L} is used in equation (3) to calculate all orientation-dependent tensors in equation (17). The position of the variables in the curly brackets determines which of the angles $\{\varphi_1, \psi, \varphi_2\}$ they replace. The angles Φ_{B} and β_{B} are tilt and azimuth angles of the direction **h** in the Cartesian crystal coordinate system that is normal to the lattice planes (hkl). The elastic property tensors are referenced in a Cartesian coordinate system which means that, in the case of non-Cartesian unit cells, the real space direction normal to the lattice planes (hkl), *i.e.* the strain 'direction' or scattering vector direction, has to be calculated. With the lattice parameters $a, b, c, \alpha, \beta, \gamma$, and using the transformation given by Sands (1995), one obtains for Φ_{B} and β_{B}

$$\Phi_{\mathrm{B}} = \arccos\left[\frac{h_z}{(h_x^2 + h_y^2 + h_z^2)^{1/2}}\right], \quad \beta_{\mathrm{B}} = \arccos\left[\frac{h_x}{(h_x^2 + h_y^2)^{1/2}}\right]. \tag{20}$$

$$\mathbf{h} = \begin{pmatrix} h_x \\ h_y \\ h_z \end{pmatrix} = \begin{bmatrix} h/a \\ -h/(a\cot\gamma) + k/(b\sin\gamma) \\ hbc\sin\alpha\,\frac{\cos\alpha\cos\gamma - \cos\beta}{V\sin\alpha\sin\gamma} + kac\sin\beta\,\frac{\cos\beta\cos\gamma - \cos\alpha}{V\sin\beta\sin\gamma} + \frac{lab\,\sin\gamma}{V} \end{bmatrix}, \tag{21}$$

where $V = abc(1 + 2\cos\alpha\cos\beta\cos\gamma - \cos^2\alpha - \cos^2\beta - \cos^2\gamma)^{1/2}$. Equation (21) assumes that $\mathbf{x}\|\mathbf{a}$, $\mathbf{y}\|(\mathbf{a}\times\mathbf{b})\times\mathbf{x}$ and $\mathbf{z}\|(\mathbf{a}\times\mathbf{b})$, where $(\mathbf{x}, \mathbf{y}, \mathbf{z})$ are the Cartesian base vectors of the transformed crystal lattice. The base vector orientation must agree with that used in the measurement of the elastic property tensors, which requires confirmation especially in the case of monoclinic and triclinic symmetry. The angle λ is the rotation angle about $\mathbf{h}$, and it runs from 0 to 2π. Generally, one has to assume that some degree of preferred grain orientation is present, which requires the use of averages weighed by the orientation distribution function (ODF) $f(g^{\rm L})$. In practical terms, both Kröner-type models, the Reuss model and the Voigt models can be written as follows (Hauk, 1997; modified Voigt: Murray & Noyan, 1999):

Kröner:

$$F_{kl} = \overline{q_{33kl}(g^{\rm L})} = \frac{\int_0^{2\pi}\left[S + t(g^{\rm L})\right]_{ijkl} m_i m_j f(g^{\rm L})\,{\rm d}\lambda}{\int_0^{2\pi} f(g^{\rm L})\,{\rm d}\lambda}; \qquad (22a)$$

Inverse Kröner:

$$F_{kl} = \overline{p^{-1}_{33kl}(g^{\rm L})} = \frac{\int_0^{2\pi}\left[C + r(g^{\rm L})\right]^{-1}_{ijkl} m_i m_j f(g^{\rm L})\,{\rm d}\lambda}{\int_0^{2\pi} f(g^{\rm L})\,{\rm d}\lambda}; \qquad (22b)$$

Voigt:

$$F_{kl} = m_i m_j \left\langle c\left(g^{\rm L}\right)\right\rangle^{-1}_{ijkl}; \qquad (22c)$$

Modified Voigt:

$$F_{kl} = m_i m_j \left[\frac{\int_0^{2\pi} c(g^{\rm L}) f(g^{\rm L})\,{\rm d}\lambda}{\int_0^{2\pi} f(g^{\rm L})\,{\rm d}\lambda}\right]^{-1}_{ijkl}; \qquad (22d)$$

Reuss:

$$F_{kl} = \frac{\int_0^{2\pi} s_{ijkl}(g^{\rm L}) m_i m_j f(g^{\rm L})\,{\rm d}\lambda}{\int_0^{2\pi} f(g^{\rm L})\,{\rm d}\lambda}. \qquad (22e)$$

Here, m_i are components of the measurement direction

$$m = (\cos\varphi\sin\psi \quad \sin\varphi\sin\psi \quad \cos\psi). \qquad (23)$$

Alternatively, in equation (22*c*), the single-crystal constants $c(g^{\rm L})$ can be replaced by matrix constants C_{ijkl} calculated using the Kröner model, which would yield a better approximation of the mechanical average. The integrations in equations (22*a*), (22*b*), (22*d*) and (22*e*) are performed numerically such that for each λ the matrix product (9) is calculated, and the Euler angles $\{\varphi_1, \phi, \varphi_2\}$ are determined from the matrix components in equation (4).

It should be emphasized that, regardless of the model used in equations (22*a*)–(22*e*), the stress factors contain no implicit statement about the stress or strain state of the grains themselves, but rather how the lattice strains change in response to changes in the macroscopic stresses. Thus, any pre-existing strains in the grains, be it from plastic anisotropy, elastic misfit or thermal expansion, are immaterial to this calculation.

3. Examples

For a discussion of examples we will focus entirely on ferritic low-alloy steel (α-iron). Because of its industrial importance this material has the most detailed body of theoretical analysis and published experimental data. This material will allow the study of the effects of preferred orientation and grain shape with good sensitivity, owing to the appreciable elastic anisotropy visible in measured lattice strain distributions, combined with high strength (large magnitude of elastic strains).

3.1. Isotropic case (no preferred orientation)

Concentrating for now on spherical grains without preferred orientation, we find that, in terms of the familiar quantities s_1 and $\frac{1}{2}s_2$, the inverse Kröner model falls between the Kröner and Reuss models (Fig. 2).

However, unlike the intersecting DECs for the Reuss and Voigt models, $\frac{1}{2}s_2$ and s_1 do not intersect for either the inverse Kröner model or the Kröner model, and one is always greater than the other. One should note that, in the case of grains in the form of aligned nonspherical ellipsoids, s_1 and $\frac{1}{2}s_2$ become dependent on (φ, ψ), and the relationship between lattice strain and macroscopic stress must be expressed by the stress factors F_{ij} in equation (1). Both models yield substantially different results if the grains are oriented such that the difference between the tensors $[c(g) - C + Cw]$ in equation (17) is large, and this is amplified by extreme grain shapes as in the case of the 100 reflection. This is shown in Fig. 3.

One must be careful not to assume that the DECs display similar symmetries to the overall or matrix elastic constants. In particular, the DECs for spherical grains ($a_1 = 1, a_2 = 1, a_3 = 1$) are not equal in both models, as predicted above in the discussion of the inequality in equation (16). This could be interpreted as placing upper and lower bounds on the DEC. However, as stated originally by Kröner [equation (8)], the tensors p and q may have interchangeable roles. In fact, the intersecting curves in Fig. 3 show that this is the case for the Kröner and inverse Kröner models, with the grain shape as the controlling factor. The asymptotic behavior of both models is particularly revealing: for grains in the form of very thin plates, the Kröner model yields stress factors that for all hkl converge to the value of the mechanical limit $F_{11}(0, 0) = -\nu/E$. Note that this value is closely related to the Voigt value but numerically different, because the matrix elastic constants were calculated using the Kröner model and not the Voigt model. The opposite behavior is found for the inverse Kröner

model: the *hkl* dependence becomes even more apparent and the model reaches the limit of values calculated by the Reuss model for each *hkl*. The stress factors in the mechanical limit for all *hkl* are calculated using equation (2) with $s_1 = \nu/E$ and $\frac{1}{2}s_2 = (1 + \nu)/E$. Poisson's ratio ν and Young's modulus E are calculated from the matrix elastic constants (Table 1). Isotropic constants are usually sufficient in accuracy (SC isotropic in Table 1), and the following formulae can be used (Hauk, 1997):

$$E = \frac{(C_{11} - C_{12})(C_{11} + 2C_{12})}{C_{11} + C_{12}} \quad \text{and} \quad \nu = \frac{C_{12}}{C_{11} + C_{12}}. \quad (24)$$

The argument presented for the asymptotic behavior of the Kröner-type models is a numerical one, *i.e.* it was inferred from the convergence of *hkl* at the extremes of elastic crystal anisotropy (100 and 111 in the cubic case) that this is the case for all *hkl*. This procedure was applied to other materials including corundum, niobium, titanium and uranium, all of which cover a wide range of crystal symmetries and elastic anisotropies. All showed the same behavior of asymptotically reaching the respective limits of the mechanical average (Kröner) and Reuss (inverse Kröner).

Table 1
Overall (matrix) elastic constants calculated using different models (GPa).

SC denotes self-consistent; SC [50,50,1] and SC [3.2,2.8,1] refer to the grain shape used.

Model	C_{11}	C_{22}	C_{33}	C_{12}	C_{13}	C_{23}	C_{44}	C_{55}	C_{66}
Voigt	294.9	293.1	297.1	114.0	110.1	111.8	86.8	85.1	90.0
Reuss	275.3	273.5	277.6	123.9	119.8	121.6	72.1	70.6	74.3
SC [50,50,1]	285.5	282.4	287.3	119.2	114.3	117.4	81.6	79.2	81.5
SC [3.2,2.8,1]	286.0	283.5	287.2	118.6	114.1	116.3	80.1	78.1	82.4
SC, isotropic	282.4	282.4	282.4	118.3	118.3	118.3	82.05	82.05	82.05

3.2. Preferred orientation

A study of the literature also shows that the Fe(211) reflection is very sensitive to the elastic effects of preferred orientation in terms of the variability of the slope $d(\sin 2\psi)$. This reflection is also one of those most frequently used in residual stress measurements on ferritic steel. In the extreme, a large tensile stress can produce d spacings that decrease with ψ in the range $\sin 2\psi = 0.2$–0.4. This reflection is therefore well suited to studying the quality of DEC model predictions.

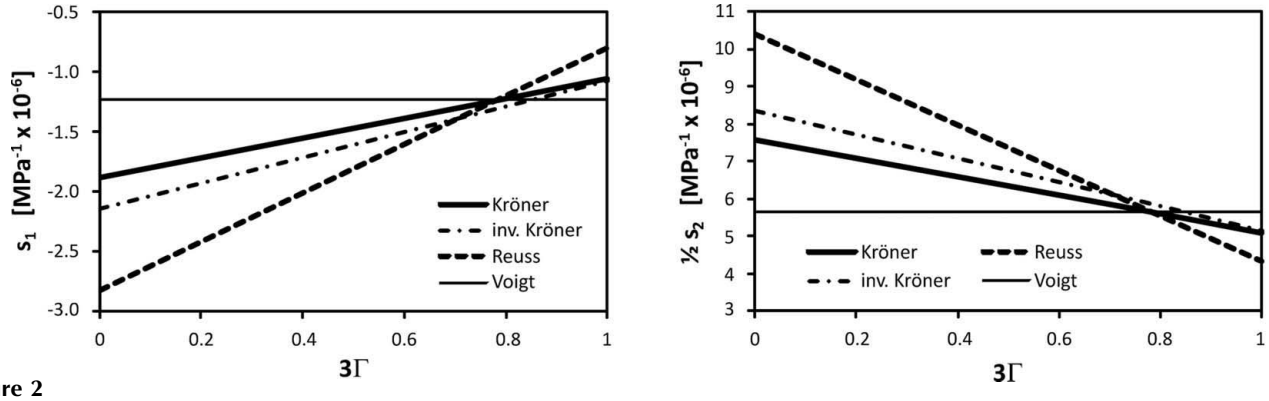

Figure 2
Diffraction elastic constants s_1 and $\frac{1}{2}s_2$ for spherical grains in an isotropic iron polycrystal over the orientation parameter $\Gamma = (h^2k^2 + h^2l^2 + k^2l^2)/(h^2 + k^2 + l^2)^2$.

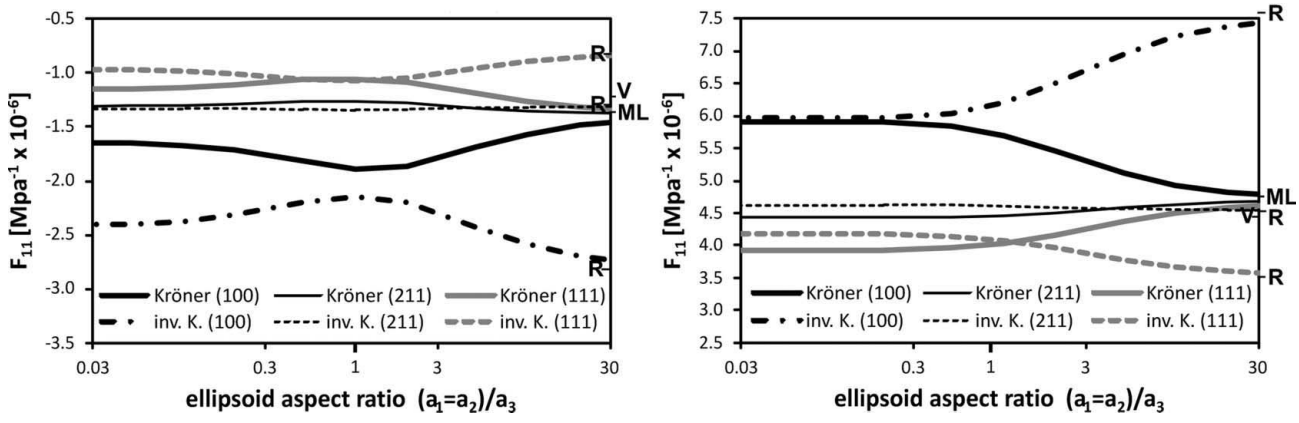

Figure 3
Calculated stress factors F_{11} for different grain shapes and reflections for an isotropic iron polycrystal in the direction **m**||ND (left) and **m**||RD (right). It is assumed that the grain ellipsoid axes align such that a_1||RD, a_2||TD and a_3||ND. R refers to the Reuss limit of the particular (*hkl*) next to it, V is the isotropic Voigt limit, and ML refers to the mechanical limit $F_{11}(0, 0) = -\nu/E$ (left) and $F_{11}(0, 90) = 1/E$ (right), where ν and E are the bulk values of Poisson's ratio and Young's modulus, respectively.

Table 2
Chemical composition of HSLA 50 in wt%; Fe provides the remainder.

C	Mn	P	S	Si	Nb
0.05	0.44	0.009	0.01	0.03	0.023

The samples used here are HSLA50 sheet metal extracted as uniaxial tensile samples (60 mm long ||RD, 5 mm wide ||TD, 0.7–1.0 mm thickness ||ND) from larger sheets of as-received material and from a sample strained to 20% in equibiaxial mode. HSLA50 is a high-strength low-alloy ferritic steel used for automotive applications. It has the composition given in Table 2.

The single-crystal elastic constants used throughout are for pure iron: c_{1111} = 237, 141 and 116 GPa (Alexandrov & Ryzhova, 1961). A second sample with the same strain history was used to extract six small plates (5 × 5 mm) to form a sample of roughly cuboidal shape for neutron diffraction pole-figure measurements of the 110, 200 and 211 reflections. This mode of operation was made necessary by the relatively small area of uniform strain on the biaxially expanded sheet sample. Also, the neutron diffraction experiments, performed at NIST (Brand *et al.*, 1997), allowed the measurement of full pole figures. The equibiaxially expanded sample was used in subsequent X-ray measurements (211 reflection, Cr $K\alpha$ radiation) under five different levels of applied stress. The as-received sheet was used to extract five tensile samples, which were stacked together in a common fixture for stress testing in a neutron diffractometer (gauge volume 3 × 3 × 5 mm) for the reflections 200, 310, 220, 211 and 222 at sample orientations (φ, ψ) of (0, 0) and (0, 90). Owing to instrumental restrictions, a more detailed scan in the tilt angle ψ was not feasible.

3.2.1. Calculations using the ODF. The pole-figure data were used in the calculation of the ODF in *MTEX* (Hielscher & Schaeben, 2008), for which the ND inverse pole figures are shown in Fig. 4.

For the subsequent calculations of DECs and overall (matrix) elastic constants, the ODF was read in textual form on a 5 × 5 × 5° grid, then expanded from the 90 × 90 × 90° range of cubic orthorhombic symmetry in the Bunge angles (φ_1, Φ, φ_2) to the full interval of 360 × 180 × 360° using symmetry operators. From this table the ODF values for a given orientation (φ_1, Φ, φ_2) were obtained through trilinear interpolation between neighboring values on the 5 × 5 × 5° grid. The cumulative effect of the numerical uncertainty from this interpolation was determined in two ways. Firstly, using the thus-read ODF, pole figures were calculated for all 24 permutations (*hkl*, *klh*, ...) of the 211 reflection, and secondly, stress factors were calculated for the same permutations. Because each *hkl* permutation results in a different but symmetry-equivalent fibre orientation **m**||**h** through Euler space, a comparison between fibres allows the quantification of the numerical accuracy of the method. The relative deviations among different permutations *hkl* for both pole figures and stress factors were of the order of 2% without bias, which was regarded as sufficiently small.

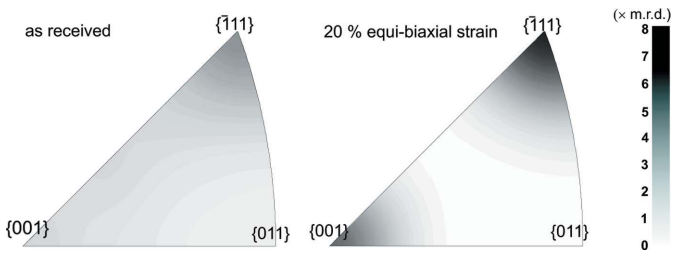

Figure 4
Inverse pole figures for ND, with levels in steps of 1 × multiples of random density (m.r.d.), for the HSLA as-received sample and after 20% equibiaxial deformation.

Equation (17) requires the rotation of the single-crystal stiffness tensor $c(g)$, for which the orientation matrix g has to be calculated in each sample direction $\mathbf{m} = (\varphi, \psi)$ using equation (19). More specifically, the numerical integration in equations (22) over discrete rotation angles λ requires the calculation of g^{L} from equation (19) for each λ, and then use of inverse trigonometric functions on the matrix elements in equation (4) to obtain the Bunge angles (φ_1, Φ, φ_2), together with the ODF value for $f(g^{\mathrm{L}})$ in equations (22).

3.2.2. Matrix elastic constants. Through equation (17) the integrations in equations (22) also require the overall or matrix elastic constants of the polycrystal. These were determined through both equations (15) using a Newton–Raphson root-finding iteration. For comparison, the upper [Voigt, equation (25*a*) below] and lower bounds [Reuss, equation (25*b*) below] on the matrix elastic constants were also calculated, with the results shown in Table 1:

$$C^{\mathrm{V}}_{ijkl} = \frac{\int_0^{2\pi}\int_0^{2\pi}\int_0^{2\pi} c_{ijkl}(g^{\mathrm{L}}) f(g^{\mathrm{L}}) \sin\Phi \, \mathrm{d}\varphi_1 \, \mathrm{d}\Phi \, \mathrm{d}\varphi_2}{\int_0^{2\pi}\int_0^{2\pi}\int_0^{2\pi} f(g^{\mathrm{L}}) \sin\Phi \, \mathrm{d}\varphi_1 \, \mathrm{d}\Phi \, \mathrm{d}\varphi_2}, \qquad (25a)$$

$$C^{\mathrm{R}}_{ijkl} = \left[\frac{\int_0^{2\pi}\int_0^{2\pi}\int_0^{2\pi} s_{ijkl}(g^{\mathrm{L}}) f(g^{\mathrm{L}}) \sin\Phi \, \mathrm{d}\varphi_1 \, \mathrm{d}\Phi \, \mathrm{d}\varphi_2}{\int_0^{2\pi}\int_0^{2\pi}\int_0^{2\pi} f(g^{\mathrm{L}}) \sin\Phi \, \mathrm{d}\varphi_1 \, \mathrm{d}\Phi \, \mathrm{d}\varphi_2} \right]^{-1}. \qquad (25b)$$

Inspection of the values in Table 1 shows that, compared with the Reuss/Voigt bounds in self-consistent (SC) estimates, the effect of both grain shape and preferred orientation on the overall elastic constants is small. Also, the SC estimates fall approximately in the middle between the Voigt and Reuss estimates. Therefore, the use of the Voigt/Reuss bounds as matrix constants should show the full extent of the matrix effect on the DECs (Fig. 5). It should be emphasized that the calculation of the matrix constants is not *per se* a necessity because one could use matrix elastic constants that were measured in some way. An example where this may be the more appropriate solution is a multiphase material where only the preferred orientation of one phase is known or measurable.

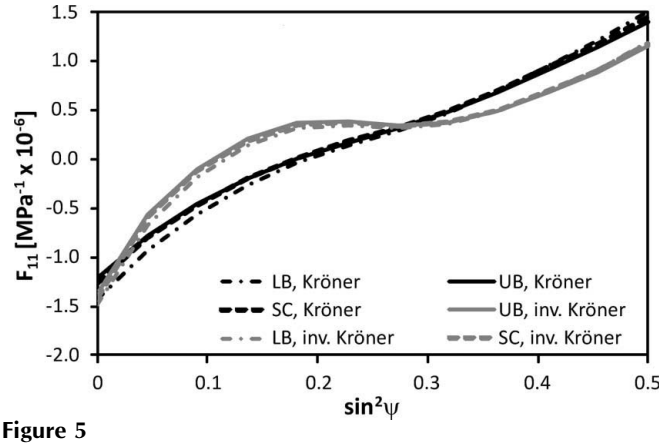

Figure 5
Effect of the matrix (overall) elastic constants on the stress factor F_{11} using the ODF of the equibiaxially expanded sample. LB stands for matrix constants calculated using the Reuss model, UB stands for the Voigt model and SC is the self-consistent estimate for the average grain shape [3.2,2.8,1]. The values are listed in Table 1.

The average grain shape of [3.2,2.8,1] was estimated using an optical intersect method for the as-received sample (average grain shape [1.85,1.6,1]) with subsequent 20% biaxial elongation in-plane and contraction in the normal direction due to volume conservation. Electron-backscatter diffraction measurements on the strained sample were not feasible because of the high dislocation density.

In the two solutions to equation (15), the differences between components $C_{ij}^{(r)} - C_{ij}^{(t)}$ are less than 0.1, and for practical purposes they are set to $C^{(r)} = CC^{(t)}$, with the result given in the table. As shown in Fig. 5, the effect of the matrix elastic constants is weak, and it has a visible effect on the diffraction stress factors only if the Voigt or Reuss bounds are used. The small differences between the SC estimates of the matrix elastic constants yield similarly small differences in the DECs, which deviate from one another by less than the line width of the SC graphs in Fig. 5.

3.2.3. Stress factors. In order to facilitate the comparison of calculated stress factors with experimental data from a plastically deformed sample, it is important to separate completely the effects of intergranular strains from the stress factor measurement. Intergranular strains, also known as residual strains of the second kind (type II), are the result of plastic deformation, and they are caused by plastic anisotropy between grains of different orientations. Intergranular strains are primarily visible in the absence of other stresses, *i.e.* under zero applied or residual stress (see Fig. 6). Thus, any effect of intergranular strains on a stress factor measurement can be completely removed by choosing the lattice strains or d spacings at zero applied load as the reference state from which, through successive application of applied stresses, the linear elastic changes are measured for each sample direction $\mathbf{m} = (\varphi, \psi)$. The actual stress factor determination is simply an application of Hooke's law, here done through the slope of the linear regression of lattice strain over applied stresses (0, 141, 249, 358 and 475 MPa) (Fig. 6, right). Note that the actual sequence should start at the highest load, with the zero load measurement as the last. This way, in the absence of creep, the stress factor measurements are guaranteed to reflect only linear elastic effects, as shown in Fig. 6, right.

Using the matrix elastic constants for SC [3.2,2.8,1] from Table 1, the F11 stress factors are calculated and compared with measurements in the ND–RD plane ($\varphi = 0^\circ$) and in the ND–TD plane ($\varphi = 90^\circ$) (Fig. 7).

For the ND–RD plane, the results reflect reports in the literature (*e.g.* Barral *et al.*, 1987; Baczmanski *et al.*, 1993) that good agreement is observed using the Reuss model, while the Kröner model generally captures less well the 'snake line' distribution of the stress factors. Of all the models, the inverse Kröner model as introduced here shows the best agreement for platelet-shaped grains with aspect ratios [50,50,1]. Using the experimentally determined estimate of the average grain shape [$a_1 = 3.2$, $a_2 = 2.8$, $a_3 = 1$], the agreement is still better than for the Kröner model. The modified Voigt model (Murray & Noyan, 1999) yields results very similar to the Reuss model. The sensitivity of the Kröner model to the grain shape is counterintuitive – needle grains aligned parallel to ND (not shown) would yield a better agreement than platelets

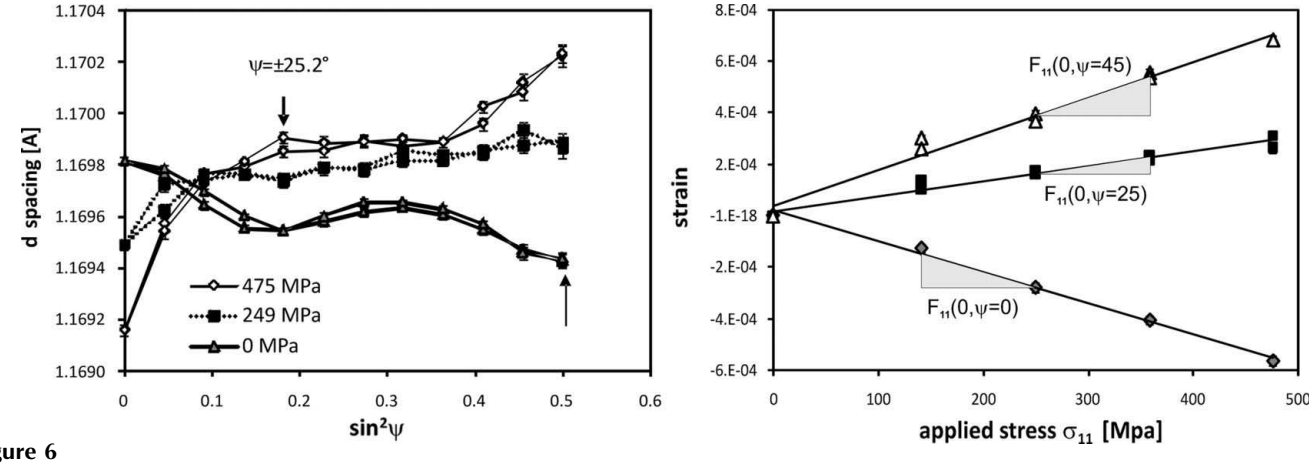

Figure 6
Left: d spacings measured for the Fe(211) reflection *versus* sin$^2\psi$ and for different applied stresses for the equibiaxially expanded sample. The specimen tilt is in the plane $\varphi = 0$ (ND–RD||stress). Right: strain $(d - d_0)/d_0$ *versus* applied stress. The reference d spacing is the value measured at zero stress (left, 0 MPa). The slopes are the values of F_{11} at $\psi = 0^\circ$, $\psi = \pm 25.2^\circ$ and $\psi = \pm 45^\circ$.

[50,50,1]. Plate-like grains with their small dimension along ND would be expected after biaxial stretching along RD and TD. The Kröner model with [50,50,1] grains approaches the mechanical limit (close to the Voigt case). In contrast, the inverse Kröner model behaves correctly, *i.e.* showing better agreement as the grain shape varies from low aspect ratios [3.2,2.8,1] to thin plates [50,50,1] where, in turn, the inverse Kröner model approaches the Reuss limit of homogeneous stress. In the ND–TD plane at $\varphi = 90^\circ$, one finds a reversal of the roles of the two models. The best agreement is now found for the Kröner model using the measurement-based estimate of the grain shape [3.2,2.8,1]. For flat grains ([50,50,1]), the Kröner model approaches the mechanical limit, just as in the ND–RD plane. Remarkably, the modified Voigt model shows similarly good agreement with the measured stress factors. The inverse Kröner model, which performed best at $\varphi = 0^\circ$ with [50,50,1] as grain-shape parameters, again approaches the Reuss limit, and both show the worst agreement. Therefore, one can surmise that this type of model agreement reflects the role of $\overline{q}_{ijkl}$ and $\overline{p}^{-1}_{ijkl}$ as bounds, as expressed in equation (8), with the grain-shape parameters controlling the proximity to the respective Reuss or mechanical limit. Even for spherical grains, the two Kröner-type models do not start out the same, but rather in close proximity to the Reuss/Voigt average (not shown), from which, on increasing the grain aspect ratio, the Kröner model approaches the mechanical limit and the inverse Kröner model approaches the Reuss limit. This is the result of the asymptotic behavior of the Eshelby tensor for a_1, $a_2 >> a_3$. Here, one has nearly homogeneous strain (grain and surrounding matrix) in the directions of a_1 (RD) and a_2 (TD), while the stresses in the a_3 direction (ND) are zero (Mura, 1987, p. 82).

It should be pointed out that grain elongation from slip due to plastic deformation depends on the orientation of the crystal lattice of the grain. For any given orientation $(\varphi, \psi)\|h$, the grains contributing to diffraction and to the integral in equation (20) will not have the same shape parameters $[a_1,a_2,a_3]$, thus making the Eshelby tensor a variable as well. This has been disregarded in this work because of the lack of appropriate data, but it provides a possible explanation of the fact that extreme ellipsoid-axes aspect ratios show the best agreement between measured and calculated stress factors in Fig. 7.

It is tempting to interpret the very good agreement of the modified Voigt model in both tilt planes (ND–RD and ND–TD) as an overall confirmation for the validity of its under-

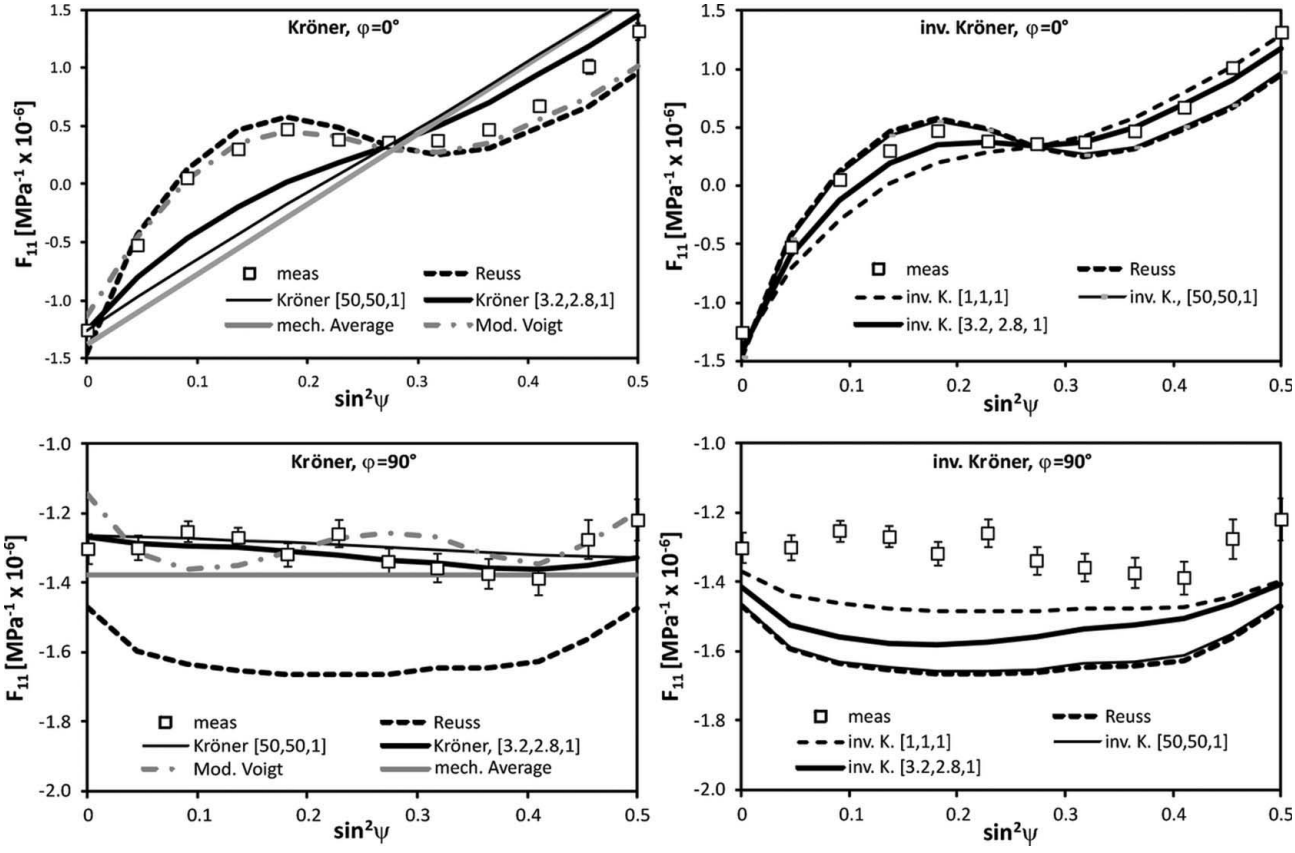

Figure 7
Comparison of measured and calculated stress factors F_{11} at $\varphi = 0^\circ$ (top) and $\varphi = 90^\circ$ (bottom) for the Kröner model (left), the inverse Kröner model (right), the mechanical average (calculated from SC [3.2,2.8,1] in Table 1), the Reuss model and the modified Voigt model. The sample was previously stretched to 20% equibiaxial strain. The direction of the applied stress was $\varphi = 0^\circ$, $\psi = 90^\circ$. The uncertainties (1σ) for the measured F_{11}, if not visible, are smaller than the size of the symbols. Orthorhombic sample symmetry (implied by the biaxial straining) was assumed and the ψ and $-\psi$ branches were averaged. The matrix constants (SC [3.2,2.8,1] in Table 1) needed in the Kröner-type models were calculated from the iron single-crystal elastic constants and the ODF using equation (25*a*).

Table 3
Stress factors F_{11} for an as-received sample of HSLA steel measured by neutron diffraction (TPa^{-1}).

χ^2 is defined as $\Sigma\left[(F_{11}^{meas} - F_{11}^{calc})^2/(F_{11}^{meas})^2\right]$. Kröner (isotropic) refers to the Kröner model with equiaxial grains and no preferred orientation. The modified Voigt, Reuss, Kröner and inverse Kröner models use the ODF, with these last two models using an average grain shape of [1.85,1.6,1].

hkl	3Γ	(φ, ψ)	F_{11}	1σ	Mechanical average	Modified Voigt	Reuss	Kröner	Inverse Kröner	Kröner (isotropic)
200	0	(0, 0)	−1.78	0.10	−1.38	−2.83	−2.83	−1.67	−2.38	−1.89
310	0.27	(0, 0)	−1.63	0.10	−1.38	−1.95	−2.36	−1.59	−2.04	−1.66
220	0.75	(0, 0)	−1.36	0.07	−1.38	−1.15	−1.46	−1.40	−1.39	−1.26
211	0.75	(0, 0)	−1.32	0.04	−1.38	−1.16	−1.49	−1.40	−1.40	−1.26
222	1	(0, 0)	−1.07	0.06	−1.38	−0.79	−0.79	−1.14	−0.98	−1.05
χ^2					0.16	0.49	0.63	0.01	0.19	0.01
200	0	(0, 90)	5.16	0.08	4.67	7.59	7.59	5.83	6.06	5.70
310	0.27	(0, 90)	4.87	0.05	4.67	5.67	6.49	5.33	5.55	5.25
220	0.75	(0, 90)	4.19	0.07	4.67	4.01	4.53	4.40	4.64	4.45
211	0.75	(0, 90)	4.28	0.08	4.67	4.02	4.53	4.45	4.58	4.45
222	1	(0, 90)	4.06	0.13	4.67	3.52	3.52	3.97	4.14	4.03
χ^2					0.05	0.27	0.36	0.03	0.07	0.02

lying assumption, *i.e.* homogeneous strain for a particular *hkl*. This is not the case, as shown by the comparison for different lattice planes (*hkl*) in Table 3, where large differences from measured values are found for the 200 and 222 reflections.

Table 3 shows, through the quality measure χ^2, that the Kröner model performs best, followed by the mechanical average which, despite its simplicity, yields roughly the same average agreement as the inverse Kröner model. Owing to the weak texture, the inclusion of the ODF into the calculation does not provide improvement over the isotropic model. All models evaluated here give similar values F_{11} for 3Γ near the mechanical average of 3Γ = 0.6 (intersect region in Fig. 2), which explains not only the good performance of the modified Voigt model for the equibiaxially strained sample, but also the general preference given in the literature to the Reuss model for mixed-type reflections such as 211. The homogeneous stress assumption of the Reuss model is clearly not justified, but the Reuss strains (which would violate continuity of displacement) it implies are small because, for the particular grain orientations involved in these reflections (such as 211), the differences $|c[(hkl)\|\mathbf{z}] - C|$ are small. For a different reason (small Voigt stress), the same applies for the Voigt model.

The results from Table 3 are applicable primarily to neutron diffraction because of the directions ($\psi = 90°$ is normally inaccessible to X-ray diffraction) and *hkl* involved. Considering the low level of preferred orientation in the as-received sample, strain measurements along the principal directions – as is typically the case in neutron diffraction – appear rather insensitive to texture. The stress factor–tilt angle dependence ($\sin^2\psi$) is more typical for X-ray diffraction, with results shown in Fig. 8. The results demonstrate that even weak texture matters in X-ray diffraction.

The differences between the two directions RD [$F_{11}(\varphi = 0°)$] and TD [$F_{22}(\varphi = 90°)$] are noticeable, with the inverse Kröner model again capturing both curves better than the Kröner model which, in turn, provides the better agreement for $F_{11}(\varphi = 90°)$ and $F_{22}(\varphi = 0°)$. In effect, this outcome is the same as for the equibiaxially expanded sample (Fig. 7).

The shape of the lattice strain distributions in Figs. 7 and 8 is determined by the texture, the grain shape and the elastic anisotropy of the grains. Because only the tilt-angle dependence of $F_{ij}(211)$ was analyzed, it would be premature to generalize the observed respective preferences for each Kröner-type model. For example, the extreme values of crystal anisotropy are represented by the 200 and 222 reflections (Table 3), and for both reflections the Kröner model is clearly the better choice. More measurements involving different material and texture combinations will be necessary to develop general criteria for the selection of a particular Kröner-type model.

4. Conclusions

A model for the calculation of diffraction stress factors, here dubbed the inverse Kröner model, has been developed and compared with measured stress factors from a sample with strong preferred orientation. In X-ray measurements of the 211 reflection, the inverse Kröner model yields the best

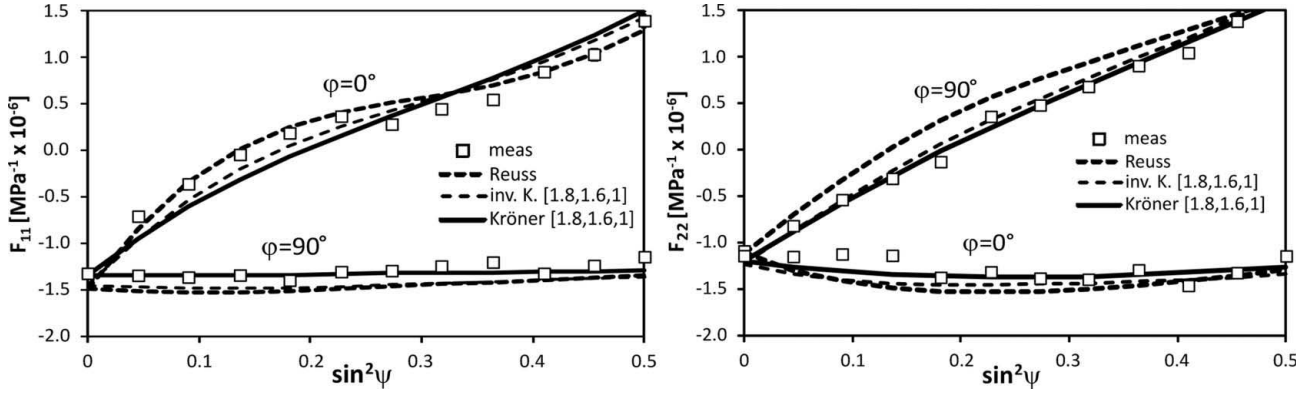

Figure 8
Measured (X-ray diffraction) and calculated stress factors F_{11} (left, measured with $\sigma_{applied}\|$RD) and F_{22} (right, measured with $\sigma_{applied}\|$TD) for the 211 reflection of the as-received sample. The Kröner and inverse Kröner model use the average grain shape [1.8,1.6,1] and the matrix elastic constants calculated from the ODF of the as-received state. The X-ray test regimen was the same as for the equibiaxially expanded sample.

agreement with measured stress factors in the tilt plane that contains the stress direction, while the Kröner model is the best choice in the tilt plane perpendicular to the stress direction. The use of elongated flat ellipsoidal grain shapes – congruent with experimental findings – is necessary to achieve this level of agreement. For extreme grain shapes, the Kröner model reaches the *hkl*-independent limit of the bulk elastic constants, while the inverse Kröner model approaches the Reuss limit. It is concluded that both models represent bounds on the diffraction elastic constants, albeit narrower than the Reuss/mechanical average limit, and with the grain shape as the controlling parameter that moves the respective Kröner-type model from a Reuss/mechanical limit average position closer to the respective bound.

For a sample with weak texture, neutron diffraction measurements of stress factors involving other *hkl* along the principal sample directions showed a general preference for the Kröner model with a negligible effect from the weak texture. However, for intermediate tilt angles typical for X-ray diffraction, even weak preferred orientation has a visible effect and it should be included in stress factor calculations.

The experimental data presented here or available in the literature are not sufficient to develop a general guideline for which model to use under a given set of circumstances (grain shape, texture). However, the large differences that are expected for *h*00-type reflections for platelet grains indicate the type of experiment necessary to gain this insight. Both models should also give different results if a realistic grain shape–crystal orientation correlation (which is a result of slip) is used.

References

Alexandrov, K. S. & Ryzhova, T. V. (1961). *Sov. Phys. Crystallogr.* **6**, 228–252.

Baczmanski, A., Wierznaowski, K., Haije, W. G., Helmholdt, R. B., Ekambaranathan, G. & Pathiraj, B. (1993). *Cryst. Res. Technol.* **28**, 229–243.

Barral, M., Lebrun, J. L., Sprauel, J. M. & Maeder, G. (1987). *Metall. Trans. A*, **18**, 1229–1238.

Behnken, H. & Hauk, V. (1986). *Z. Metallkd.* **77**, 620–626.

Bollenrath, F., Hauk, V. & Müller, E. H. (1967). *Z. Metallkd.* **58**, 76–82.

Brakman, C. M. & Penning, P. (1988). *Acta Cryst.* A**44**, 163–167.

Brand, P. C., Prask, H. J. & Gnäupel-Herold, T. (1997). *Physica B*, **241–243**, 1244–1245.

Bunge, H.-J. (1982). *Texture Analysis in Materials Science*. London: Butterworth.

Dölle, H. (1979). *J. Appl. Cryst.* **12**, 489–501.

Dölle, H., Hauk, V. & Zeegers, H. (1977). *J. Strain Anal.* **12**, 62–65.

Dölle, H., Hauk, V. & Zeegers, H. (1978). *Z. Metallkd.* **69**, 766–772.

Eshelby, J. D. (1961). *Elastic Inclusions and Inhomogeneities*. *Progress in Solid Mechanics*, Vol. II, pp. 88–140. Amsterdam: North-Holland.

Gavazzi, A. C. & Lagoudas, D. C. (1990). *Comput. Mech.* **7**, 13–19.

Hauk, V. (1997). *Structural and Residual Stress Analysis by Nondestructive Methods*. Amsterdam: Elsevier Science.

Hielscher, R. & Schaeben, H. (2008). *J. Appl. Cryst.* **41**, 1024–1037.

Hill, R. (1952). *Proc. Phys. Soc. London*, **65**, 349–354.

Kinoshita, N. & Mura, T. (1971). *Phys. Status Solidi. (a)*, **5**, 759–768.

Kneer, G. (1965). *Phys. Status Solidi*, **9**, 825–838.

Koch, N., Welzel, U., Wern, H. & Mittemeijer, E. (2004). *Philos. Mag.* **84**, 3547–3570.

Kröner, E. (1958). *Z. Phys.* **151**, 504–518.

Matthies, S. & Humbert, M. (1993). *Phys. Status Solidi. (b)*, **177**, K47–K50.

Möller, H. & Martin, G. (1939). *Mitt. Kaiser Wilhelm Inst. Eisenforsch. Duesseldorf*, **21**, 261–269.

Moraviec, A. (1989). *Phys. Status Solidi (b)*, **154**, 535–541.

Mura, T. (1987). *Micromechanism of Defects in Solids*, ch. 3. Dordrecht: Martinus Nijhoff Publishers.

Murray, C. E. & Noyan, I. C. (1999). *Philos. Mag. A*, **79**, 371–389.

Ortner, B. (2006). *J. Appl. Cryst.* **39**, 401–409.

Pina, J., Dias, A., François, M. & Lebrun, J. L. (1997). *Surf. Coat. Technol.* **96**, 148–162.

Sands, D. E. (1995). *Vectors and Tensors in Crystallography*. New York: Dover Publications.

Van Houtte, P. & De Buyser, L. (1993). *Acta Metall. Mater.* **41**, 323–336.

Wit, R. de (1997). *J. Appl. Cryst.* **30**, 510–511.